Supporting information

Water-mediated kinetic engineering of CTF QDs for emerging solar cells

Manying Liu,*[a] Zikang Lei,[a] Peiyuan Ma,[a] Lixin Feng,[a] Yuanhao Wang,[a] Dandan Zhao,[a] Yanru Guo,[a] Yange Zhang,[a] Xin Zhao,*[b] and Zhi Zheng*[a]

[a]Key Laboratory of Micro-Nano Materials for Energy Storage and Conversion of Henan Province, Institute of Surface Micro and Nano Materials, College of Chemical and Materials Engineering, Xuchang University, Henan 461000, China.

E-mail: manyingliu988@xcu.edu.cn, zzheng@xcu.edu.cn

[b]State Key Laboratory of Organometallic Chemistry, Shanghai Institute of Organic Chemistry, Chinese Academy of Sciences, Shanghai 200032, China.

E-mail: xzhao@sioc.ac.cn

Keywords: covalent triazine frameworks, quantum dots, kinetics, interfacial modifier, solar cells

Section 1 Materials, Characterizations, and Methods

Materials: All chemical reagents were employed as received without additional purification. Anhydrous dimethyl sulfoxide (DMSO), benzene-1,4-dicarbonitrile, N,N-dimethylformamide (DMF, anhydrous grade), terephthalaldehyde, potassium tert-butoxide, and 2,5-thiophenedicarboxaldehyde were procured from Shanghai Adamas Reagent Co., Ltd. Terephthalamidine was synthesized in-house following established protocols.[1] Fluorine-doped tin oxide (FTO) conductive glass substrates (1.5 × 1.5 cm^2, 8 Ω/sq) were acquired from Shanghai Zaofu New Materials Co., Ltd. High-purity cesium bromide (CsBr, 99.99%) and lead bromide ($PbBr_2$, 99.9%) were sourced from Macklin Biochemical Co., Ltd.

Synthetic procedures of CTF QDs: Taking CTF-QD-1 as an example, the synthesis process is described below. First, 0.1632 g (1.0 mmol) of terephthalamidine was dissolved in 3 mL of deionized water and heated to 50°C with stirring until fully dissolved. Then, this terephthalamidine solution, along with 0.0675 g (0.5 mmol) of terephthalaldehyde and 0.1683 g (1.1 mmol) of potassium tert-butoxide, were added to a 50 mL round-bottom flask. Following this, 10 mL of DMF was introduced, and the mixture was thoroughly shaken to ensure homogeneity. The reaction proceeded in a microwave reactor (1500 W, 50%) for 55 minutes, resulting in the CTF-QD-1 solution. After completion, the mixture was cooled, washed with dilute hydrochloric acid, and centrifuged at 10000 rpm. Finally, the product was freeze-dried to yield 0.0566 g of a light-yellow powder, corresponding to a yield of 27.6%. CTF-QD-2 was synthesized using an identical procedure, substituting 0.0700 g (0.5 mmol) of 2,5-thiophenedicarboxaldehyde for the terephthalaldehyde, resulting in a yield of 28.4%.

Synthesis of SnO_2 QDs: SnO_2 quantum dots were prepared by dissolving 1.015 g of $SnCl_2{\cdot}2H_2O$ and 0.335 g of CH_4N_2S in 30 mL of deionized water in an uncovered beaker. The resulting slightly opaque, pale-yellow mixture was continuously stirred magnetically at room temperature for 36 hours. Following stirring, the mixture was

centrifuged at 9000 rpm for 5 minutes and filtered through a 0.22 µm PTFE membrane to yield a transparent yellow solution of SnO_2 quantum dots.

Fabrication of Carbon-Based $CsPbBr_3$ Perovskite Solar Cells (PSCs): Pristine $CsPbBr_3$ PSCs were fabricated following a reference methodology.[2] FTO substrates underwent sequential cleaning with detergent, acetone, isopropanol, ethanol, and DI water, followed by UV-ozone treatment for 30 minutes to ensure surface decontamination. A SnO_2 quantum dot electron transport layer (ETL) was uniformly spin-coated (2000 rpm, 30 s) onto the FTO substrate and thermally cured at 200°C for 1 hour under ambient conditions. A preheated (80°C) 1 M $PbBr_2$ solution in DMF was then spin-coated (2000 rpm, 30 s) onto the FTO/ETL substrate and annealed at 90°C for 30 minutes. This process was followed by spin-deposition (2000 rpm, 30 s) of a 0.07 M CsBr methanol solution onto the $PbBr_2$ layer, which was then sintered at 250°C for 5 minutes. This sequential coating and annealing cycle were repeated 9 times to achieve the desired perovskite film. The device fabrication concluded with blade-coating a carbon electrode onto the FTO/ETL/$CsPbBr_3$ stack.

For $CsPbBr_3$@CTF-QD-1 PSCs, the protocol was modified by integrating CTF-QD-1 films at varying concentrations (1.0, 2.0, and 3.0 mg/L) into the $PbBr_2$ precursor solution prior to deposition. All other procedural parameters remained unchanged.

Characterizations: The chemical structure of CTF QDs was characterized using Fourier-transform infrared (FT-IR) spectroscopy (Bruker Vertex 70), X-ray photoelectron spectroscopy (XPS) on an Axis Ultra DLD 600 W instrument (Shimadzu, Japan), and ^{13}C cross-polarization magic-angle spinning nuclear magnetic resonance (^{13}C CP/MAS NMR, 400 MHz WB Bruker Avance II). The porous characteristics of CTF QDs were investigated with a surface area and porosity analyzer (Micromeritics ASAP 2020 M), where pore size distribution was determined through non-local density functional theory (NLDFT) modeling using N_2 adsorption-desorption isotherms. The crystallinity of CTF QDs and $CsPbBr_3$ was analyzed by X-ray diffraction (XRD, Philips X'Pert Pro) with

Cu Kα radiation (λ = 1.5418 Å). Morphological features of CTF QDs were investigated through field-emission scanning electron microscopy (FE-SEM, FEI Sirion 200) and transmission electron microscopy (TEM, Tecnai G2 F30, FEI Holland). UV-vis-NIR absorption spectra were acquired using a Cary 5000 spectrophotometer (Varian). Steady-state photoluminescence (PL) and time-resolved photoluminescence (TRPL) measurements were performed with a fluorescence spectrophotometer (excitation wavelength: 465 nm). Transient surface photovoltage (TSPV) signals were recorded under 355 nm pulsed laser excitation. Current density-voltage (*J*-*V*) characteristics were evaluated under ambient conditions using a solar simulator with AM 1.5G illumination (100 mW/cm^2).

Section 2 Fig. S1-S16 and Tables S1-S4

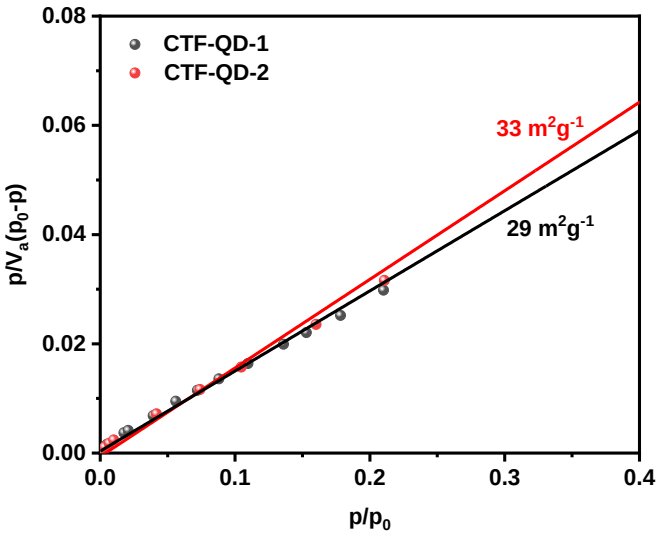

Fig. S1 Brunauer-Emmett-Teller (BET) analysis plots of CTF-QDs.

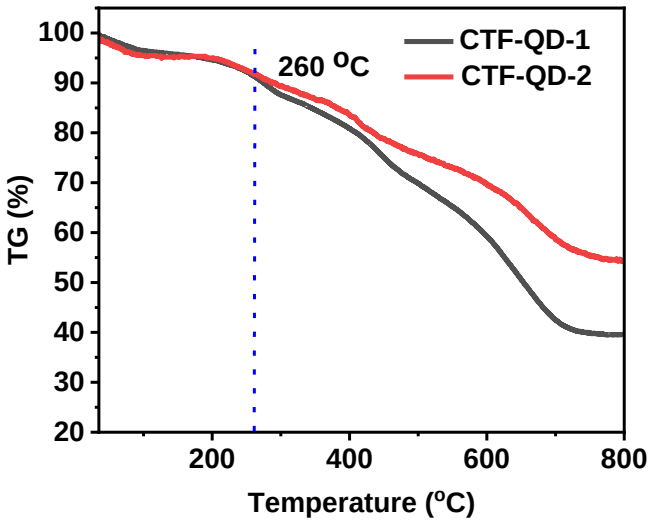

Fig. S2 Thermogravimetric (TG) analysis of CTF-QDs

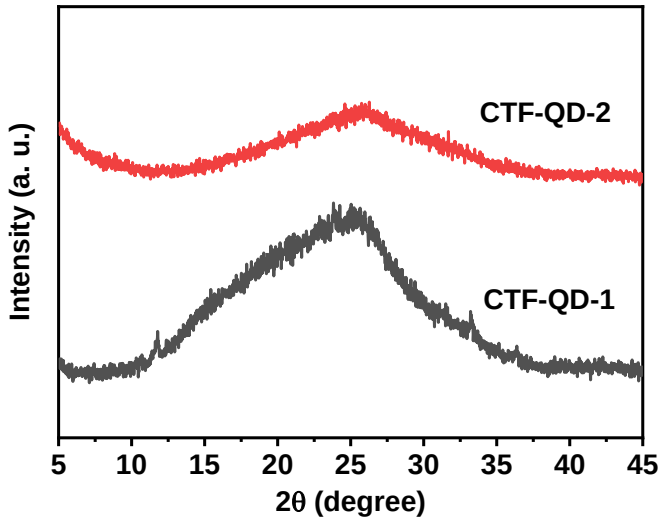

Fig. S3 XRD patterns of CTF-QD-1 and CTF-QD-2

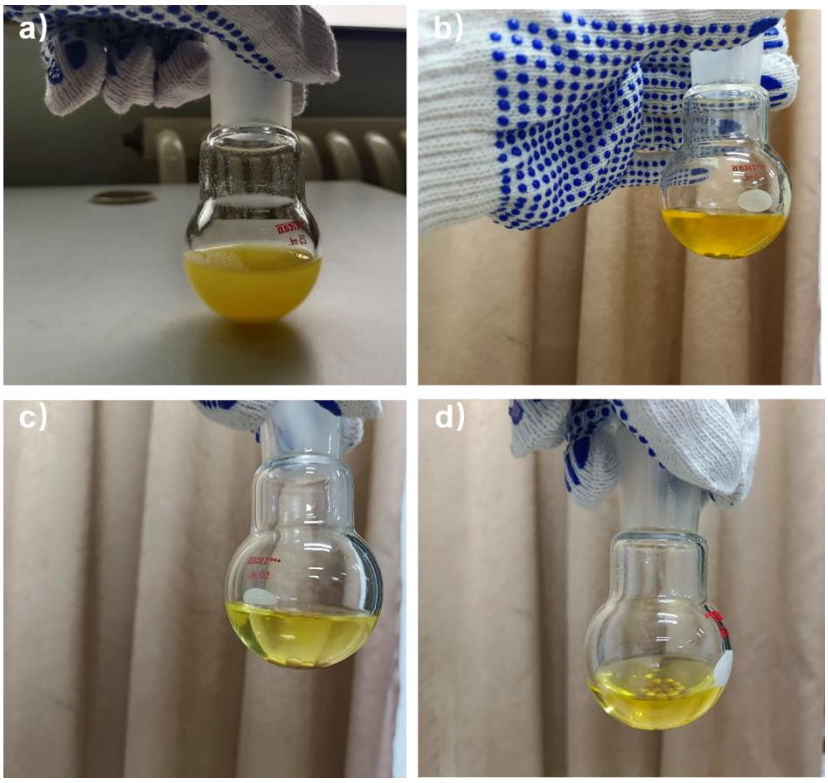

Fig. S4 Digital photos of CTF-QD-1 with different amounts of water added during the polymerization reaction: (a) 1 mL, (b) 2 mL, (c) 3 mL, and (d) 4 mL.

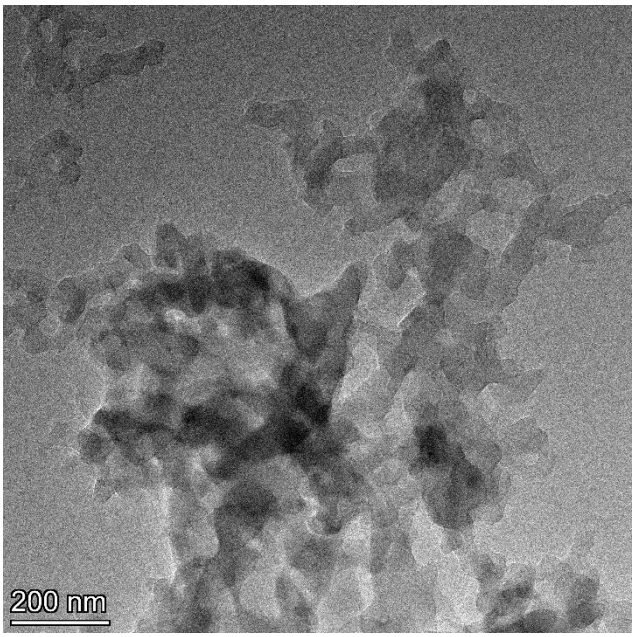

Fig. S5 TEM image of CTF-QD-1 obtained upon the addition of 0 mL water.

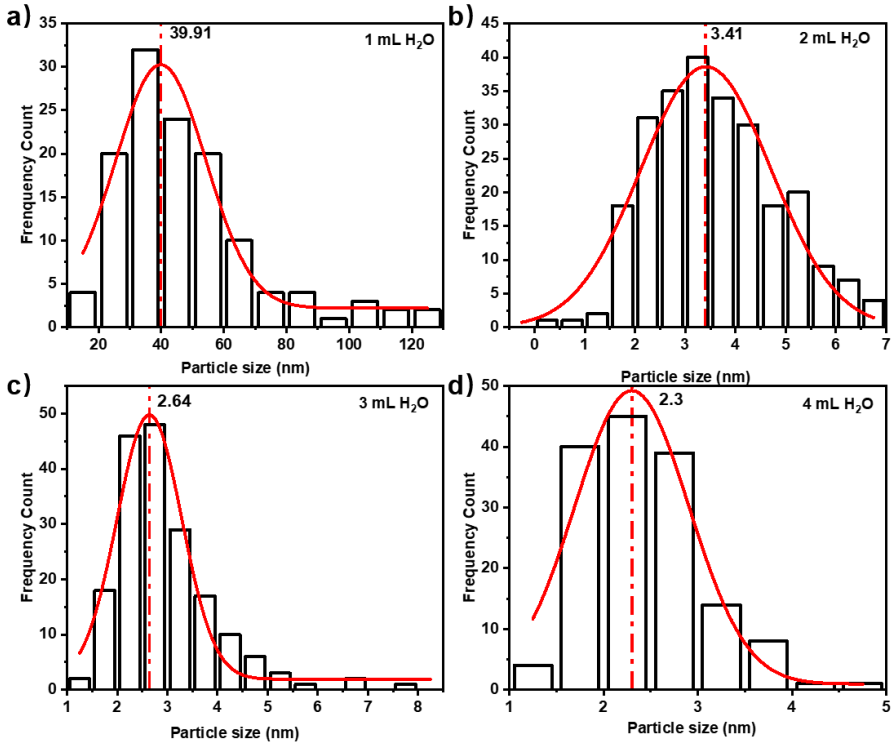

Fig. S6 Particle size distributions characterized through statistical analysis of high-resolution TEM micrographs using ImageJ software with the addition of (a) 1 mL, (b) 2 mL, (c) 3 mL, and (d) 4 mL water.

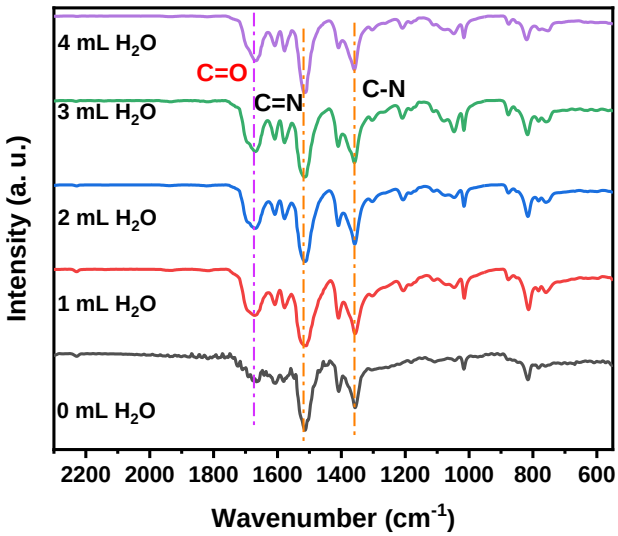

Fig. S7 Normalized FT-IR Spectra for CTF-QD-1 with varying water dosages.

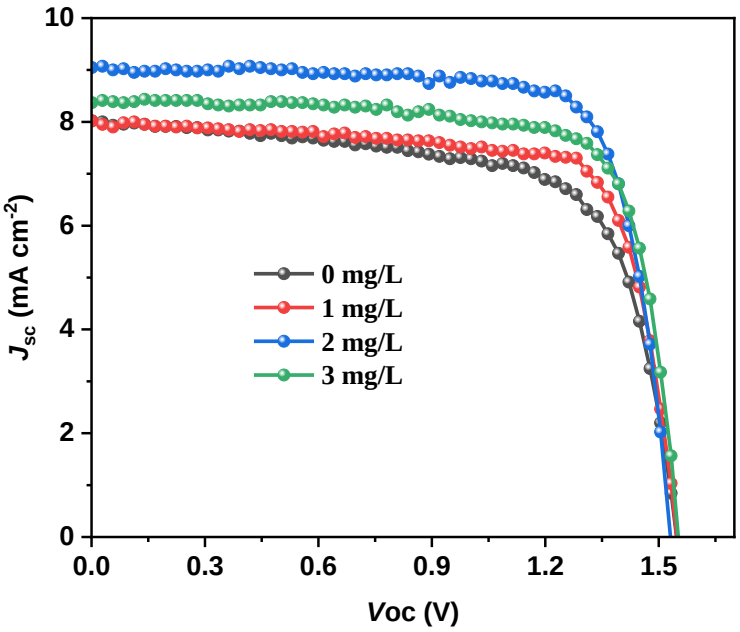

Fig. S8 *J–V* curves of $CsPbBr_3$ PSCs with different CTF-QD-1 concentrations.

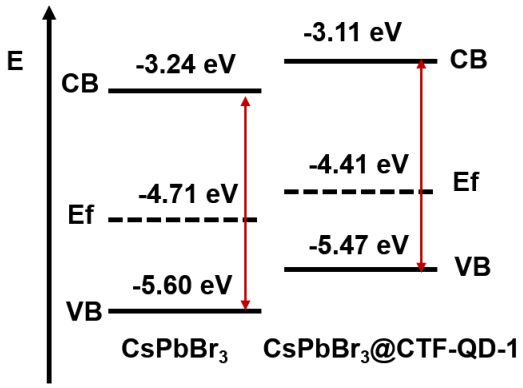

Fig. S9 Schematic of energy level diagram of $CsPbBr_3$ and $CsPbBr_3$@CTF-QD-1.

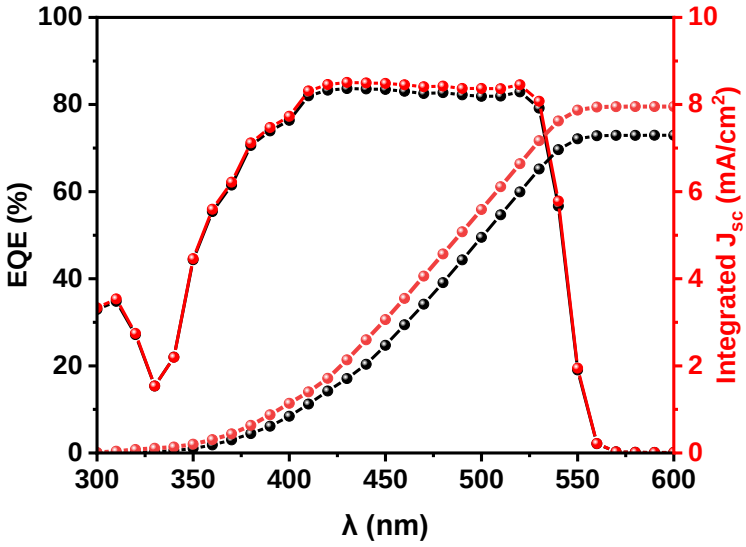

Fig. S10 EQE curves of $CsPbBr_3$ (black) and $CsPbBr_3$@CTF-QD-1(red) PSCs.

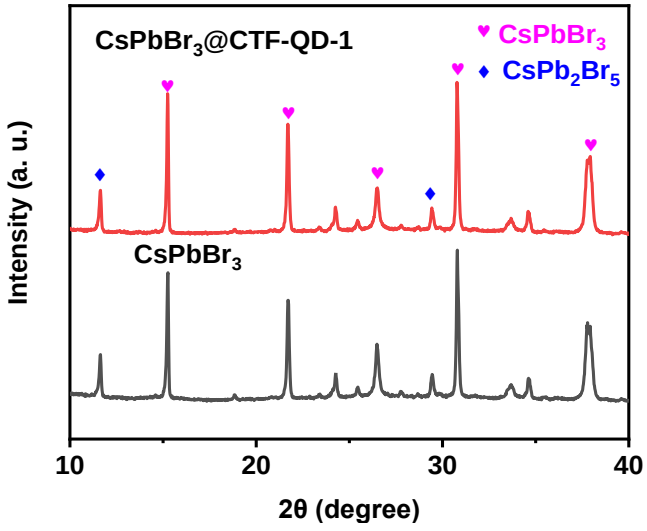

Fig. S11 XRD patterns of $CsPbBr_3$ and $CsPbBr_3$@ CTF-QD-1.

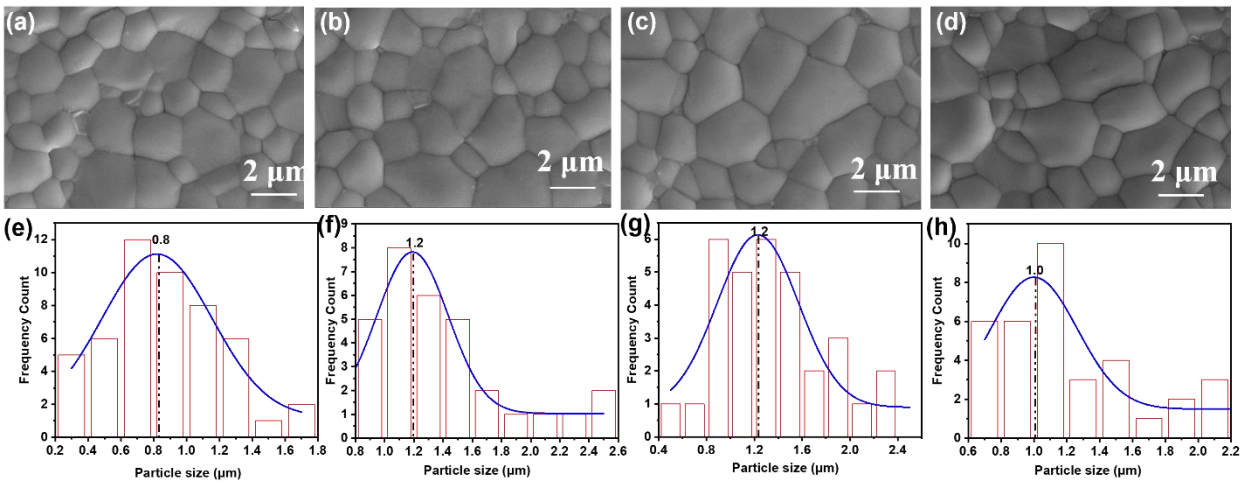

Fig. S12 SEM images and particle size distribution statistical analyses of $CsPbBr_3$ with the addition of CTF-QD-1 are shown for the following concentrations: (a) and (e) 0 mg/L, (b) and (f) 1.0 mg/L, (c) and (g) 2.0 mg/L, and (d) and (h) 3.0 mg/L, respectively.

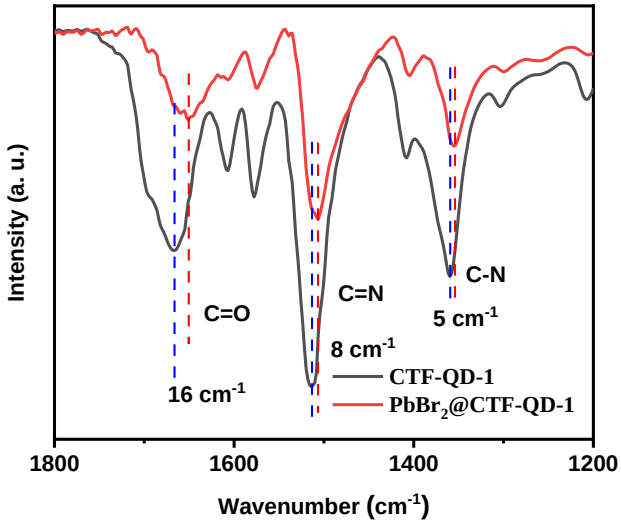

Fig. S13 FT-IR spectra of CTF-QD-1 and $PbBr_2$@CTF-QD-1.

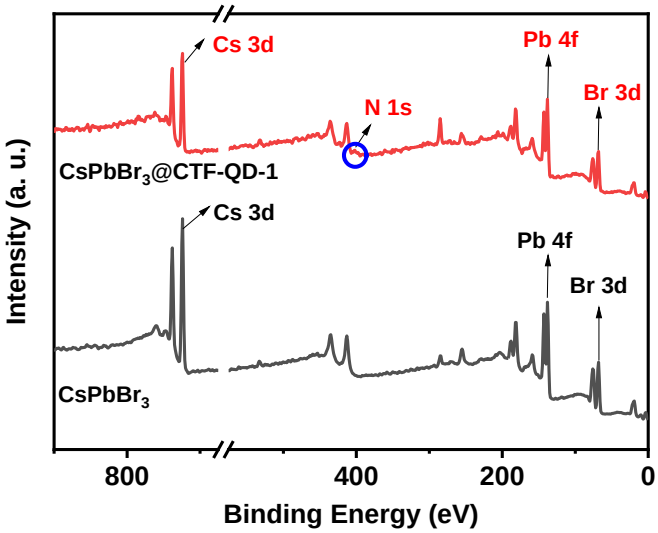

Fig. S14 XPS survey spectra of $CsPbBr_3$ and $CsPbBr_3$@CTF-QD-1.

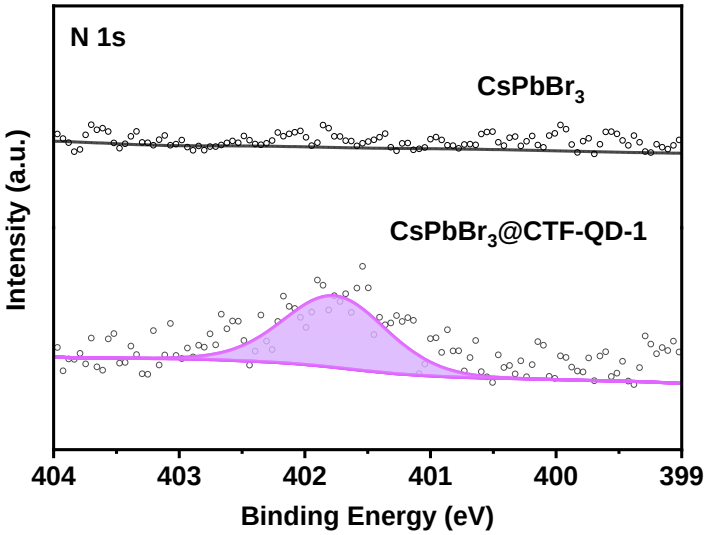

Fig. S15 XPS spectra of N 1s core level of $CsPbBr_3$ and $CsPbBr_3$@CTF-QD-1.

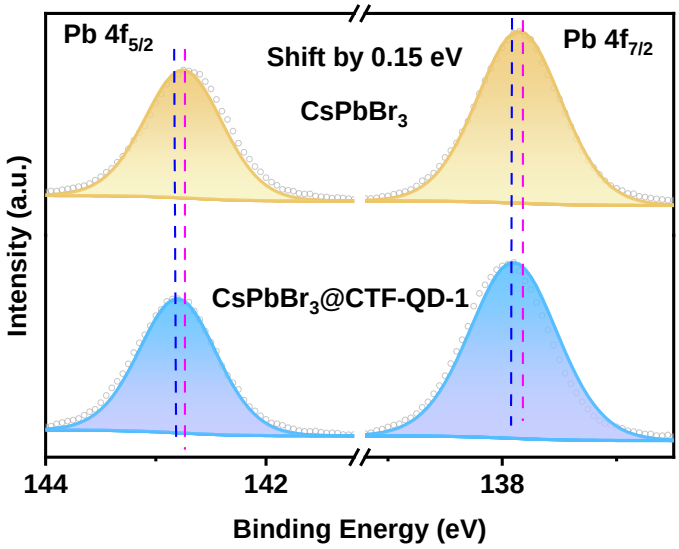

Fig. S16 XPS spectra of Pb 3d core level of $CsPbBr_3$ and $CsPbBr_3$@CTF-QD-1.

Table S1 Element analysis of CTF-QDs.

Sample	N (Wt%)	C (Wt%)	H (Wt%)	S (Wt%)	O (Wt%)
CTF-QD-1	12.14	58.88	6.08	0.00	22.90
CTF-QD-2	12.96	53.73	3.78	7.54	21.99

Table S2 Photovoltaic parameters of $CsPbBr_3$ PSCs with different CTF-QD-1 concentrations.

Concentration of CTF-QD-1	V_{oc}/(V)	J_{sc}/(mA/cm^2)	FF/(%)	PCE/(%)
0mg/L	1.55	7.96	68.30	8.40
1 mg/L	1.55	7.97	75.30	9.27
2 mg/L	1.56	9.49	74.57	11.01
3 mg/L	1.55	8.39	75.90	9.87

Table S3 TSPV parameters of $CsPbBr_3$ and $CsPbBr_3$@ECTF-1 films.

Sample	T_t (s)	T_r (s)	L
$CsPbBr_3$	7.12×10^{-7}	2.27×10^{-5}	3.14×10^{-2}
$CsPbBr_3$@CTF-QD-1	7.12×10^{-7}	6.14×10^{-5}	1.16×10^{-2}

Table **S4** Photovoltaic parameters comparison of state-of-the-art $CsPbBr_3$ perovskite solar cells.

PSCs	PCE (%)	J_{sc}(mA cm^2)	V_{oc}（V)	FF（%）	Ref.
FTO/SnO_2/$CsPbBr_3$@CTF-QD-1/Carbon	11.01	9.49	1.560	74.57	This work
FTO/SnO_2-$TiOxCl_{4-2x}$/$CsPbBr_3$+$Ti_3C_2Cl_x$/$Ti_3C_2Cl_x$/Carbon	11.08	7.87	1.702	82.7	a[3]
FTO/c-TiO_2/m-TiO_2/$CsPbBr_3$/ $CuInS_2$/ZnS QDs/LPP-Carbon	10.85	7.73	1.626	86.3	b[4]
FTO/TiO_2/DTPT/$CsPbBr_3$/DTPT/Carbon	11.21	8.52	1.574	83.67	c[5]
FTO/c-TiO_2/m-TiO_2/$CsPbBr_3$/ DCC/Carbon	10.16	7.79	1.611	80.96	d[6]
FTO/c-TiO_2/m-TiO_2/$CsPbBr_3$/(WS_2/$AgIn_5S_8$) QDs HTM/Carbon	10.24	7.49	1.627	84.03	e[7]
FTO/c-TiO_2/m-TiO_2/$CsPbBr_3$/VO@CNF	8.80	8.86	1.289	77.0	f[8]
FTO/c-TiO_2/m-TiO_2/Sm^{3+}-$CsPbBr_3$/ Cu(Cr,Ba)O_2/Carbon	10.79	7.81	1.615	85.5	g[9]
FTO/c-TiO_2/PTl-$CsPbBr_3$/spiro-OMeTAD/Ag	10.91	9.78	1.498	74.47	h[10]
FTO/c-TiO_2/$CsPbBr_3$/Carbon	9.35	7.37	1.545	82.2	i[11]
FTO/c-TiO_2/m-TiO_2/ $CsPb_{0.97}Tb_{0.03}Br_3$/SnS:ZnS/NiO_x/carbon	10.26	8.21	1.57	79.6	j[12]
FTO/SnO_2/$CsPbBr_3$/N-CQDs/Carbon	10.71	7.87	1.622	80.1	k[13]
FT0/$Sn0_2$/$CsPbBr_3$/$CsSnBr_2$/Carbon	10.60	7.80	1.610	84.4	l[14]
FTO/SnO_2-TiO_xCl_{4-2x}/WS_2/CsPbBr3/Carbon	10.65	7.95	1.70	79	m[15]
FTO/c-TiO_2/m-TiO_2/Sm^{3+}-$CsPbBr_3$/Carbon	10.14	7.48	1.594	85.1	n[16]
FTO/SnO_2/$CsPbBr_3$-DPPP/Carbon	11.23	7.88	1.707	83.48	O[17]

References

1. M. Liu, Q. Huang, S. Wang, Z. Li, B. Li, S. Jin and B. Tan, *Angew. Chem. Int. Ed.*, 2018, **57**,

11968-11972.

2. Y. He, Z. Li, M. Liu, S. Liu, J. Fu, Y. Zhang, Q. Li, Y. Tong and Z. Zheng, *Dalton Transactions*, 2023, **52**, 17308-17314.

3. Q. Zhou, J. Duan, J. Du, Q. Guo, Q. Zhang, X. Yang, Y. Duan and Q. Tang, *Adv. Sci.*, 2021, **8**, 2101418.

4. J. Duan, Y. Wang, X. Yang and Q. Tang, *Angew. Chem. Int. Ed.*, 2020, **59**, 4391-4395.

5. R. Guo, J. Xia, H. Gu, X. Chu, Y. Zhao, X. Meng, Z. Wu, J. Li, Y. Duan, Z. Li, Z. Wen, S. Chen, Y. Cai, C. Liang, Y. Shen, G. Xing, W. Zhang and G. Shao, *J. Mater. Chem. A*, 2023, **11**, 408-418.

6. J. Zhu, Y. Liu, B. He, W. Zhang, L. Cui, S. Wang, H. Chen, Y. Duan and Q. Tang, *Chem. Eng. J.*, 2022, **428**, 131950.

7. H. Sui, B. He, J. Ti, S. Sun, W. Jiao, H. Chen, Y. Duan, P. Yang and Q. Tang, *Chem. Eng. J.*, 2023, **455**, 140728.

8. X. Wang, Y. Gao, J. Guo and M. Wu, *Carbon*, 2024, **230**, 119566.

9. J. Duan, Y. Zhao, Y. Wang, X. Yang and Q. Tang, *Angew. Chem. Int. Ed.*, 2019, **58**, 16147-16151.

10. G. Tong, T. Chen, H. Li, L. Qiu, Z. Liu, Y. Dang, W. Song, L. K. Ono, Y. Jiang and Y. Qi, *Nano Energy*, 2019, **65**, 104015.

11. T. Xiang, Y. Zhang, H. Wu, J. Li, L. Yang, K. Wang, J. Xia, Z. Deng, J. Xiao, W. Li, Z. Ku, F. Huang, J. Zhong, Y. Peng and Y.-B. Cheng, *Sol. Energy Mater. Sol. Cells*, 2020, **206**, 110317.

12. H. Yuan, Y. Zhao, J. Duan, Y. Wang, X. Yang and Q. Tang, *J. Mater. Chem. A*, 2018, **6**, 24324-24329.

13. Y. Zhao, J. Duan, Y. Wang, X. Yang and Q. Tang, *Nano Energy*, 2020, **67**, 104286.

14. Y. Zhao, J. Duan, H. Yuan, Y. Wang, X. Yang, B. He and Q. Tang, *Solar RRL*, 2019, **3**, 1800284.

15. Q. Zhou, J. Duan, X. Yang, Y. Duan and Q. Tang, *Angew. Chem. Int. Ed.*, 2020, **59**, 21997-22001.

16. J. Duan, Y. Zhao, X. Yang, Y. Wang, B. He and Q. Tang, *Adv. Energy Mater.*, 2018, **8**, 1802346.

17. Y. Teng, Y. Zhao, Z. Xin, L. Bian, Q. Guo, J. Duan, J. Dou, Y. Zhang, Q. Zhang and Q. Tang, *J. Mater. Chem. A*, 2025, **13**, 21493-21500.